



# Predictive models for daylight performance of general floorplans based on CNN and GAN: A proof-of-concept study

Qiushi He<sup>a,c</sup>, Ziwei Li<sup>b</sup>, Wen Gao<sup>a</sup>, Hongzhong Chen<sup>a,c</sup>, Xiaoying Wu<sup>a,c</sup>, Xiaoxi Cheng<sup>a</sup>, Borong Lin<sup>a,c,\*</sup>

<sup>a</sup> Department of Building Science, School of Architecture, Tsinghua University, Beijing 100084, China

<sup>b</sup> College of Architecture & Urban Planning, Beijing University of Technology, Beijing 100124, China

<sup>c</sup> Key Laboratory of Eco Planning & Green Building, Ministry of Education, Tsinghua University, China

## ARTICLE INFO

### Keywords:

Daylight prediction  
Proxy model  
Convolutional neural network (CNN)  
Generative adversarial network (GAN)

## ABSTRACT

A daylight performance evaluation at the early design stage is essential for a building morphology design and optimization, having a tremendous influence on energy consumption and indoor environments. Considering the complicated input parameters, time and computational cost of the simulation tools, although proxy models based on various machine learning algorithms have been developed, they are limited to certain building forms described based on the selected parameters. In this study, proxy models of a daylight simulation for general floorplans are proposed based on convolutional neural network (CNN) and generative adversarial network (GAN). ResNet (CNN) and pix2pix (GAN) are applied to predict static and annual daylight metrics (uniformity, mean lux, success rate, sDA, and UDI) and illuminance distribution in space, respectively. Geometry information is embedded in the image structure, and a grid-based simulation are conducted as the ground truth. Two datasets composed of real floorplan cases and parametric rooms were tested in the experiments. ResNet obtains the best  $R^2$  of 0.959 and an MSE of 0.008 on the real case dataset for daylight uniformity. In addition, pix2pix generates visualization results close to the simulation with an SSIM of 0.90 in the test set within a period of 1 s and provides real-time intuitive feedback for designers. The results show the possibility of using deep neural networks to extract features from general building forms and build predictive models, which can be integrated into automatic form-finding and design optimization.

## 1. Introduction

### 1.1. Background

Climate change and the energy crisis have brought constant attention to building energy consumption and CO<sub>2</sub> emissions [1,2]. At the same time, the requirements for a healthy and comfortable indoor environment continue to increase. Therefore, for building performance optimization, both the energy efficiency and indoor environment quality should be considered [3]. Adequate natural daylight inside buildings can help to reduce energy consumption by substituting artificial lighting [4]. In addition, natural daylight can provide non-visual effects leading to healthy and efficient light environments that are difficult to achieve using only artificial equipment [5,6]. The building morphology is determined at the early design stage and has a tremendous influence on building daylight performance [7,26]. Therefore, a daylight

performance prediction and evaluation are essential for building design and optimization.

Generally, the simulation and proxy models are the two main daylight prediction methods during the early design stage. Validated simulation tools are widely accepted and applied in daylight performance evaluations [8–10]. The simulation calculations are based on mechanism and called white-box models. Such models require comprehensive input parameters, provide accurate results, and are compatible with most building forms. The two main categories of physically based lighting simulation algorithms are ray tracing and radiosity, and both contain large scale matrix operations depending on time and space resolution. Various efforts have been made to speed up the simulations through algorithm simplification and hardware acceleration, which made it acceptable for design evaluation [11–16]. However, building forms are modified and optimized iteratively at the early design stage, and the simulation models have to be changed

\* Corresponding author. Department of Building Science, School of Architecture, Tsinghua University, Beijing 100084, China.

E-mail addresses: [hqs18@mails.tsinghua.edu.cn](mailto:hqs18@mails.tsinghua.edu.cn) (Q. He), [linbr@tsinghua.edu.cn](mailto:linbr@tsinghua.edu.cn) (B. Lin).

accordingly, so running simulations can be time consuming. In addition, not all parameters involved in the simulation are changeable or need to be determined at this stage like materials, and accurate calculations can be time and calculation consuming [17]. Therefore, a faster prediction model with fewer input parameters is needed; hence, proxy models based on algorithms are an alternative method for daylight prediction [19,35]. Machine learning (ML) based proxy models, called black-box models, learn from data to depict non-linear relationships between input parameters and output metrics, and facilitate design evaluation [18]. Rather than selecting all detailed parameters, proxy models only select important and changeable parameters as input and are particularly efficient for an iterative optimization [19]. Nevertheless, common problems of proxy models include feature selection and model transfer. The Geometric features described by the selected parameters are restricted to certain forms, such as a box, and cannot be transferred to handle different forms. Therefore, a new method between detailed simulations and parametric proxy models that is compatible with various building forms and achieves a fast prediction with fewer parameters can better fulfill the requirements for a design optimization.

Artificial intelligence technologies have developed rapidly in recent years and have been deployed in various areas including medical care, public security and autonomous vehicles, providing inspiration for new methods for daylight proxy models. Computer vision (CV) is one of the main research directions for which deep convolutional neural networks have achieved success. The performance of the algorithm can be close to that of humans in image processing tasks, such as image classification, image segmentation, and object detection [20,21]. In a daylight simulation and prediction, reference planes are evenly divided into grids and become array data, similar to an image structure composed of pixels, which makes it possible to apply such networks to daylight prediction. Deep learning methods comprise multiple levels of representation and learn complex functions. Convolutional neural networks (CNNs) are a class of large learning capacity models that make strong and mostly correct assumptions about the nature of images and use fewer connections and parameters than feedforward neural networks [22]. They can help extract features from a general geometry and construct non-linear models to predict the overall daylight performance metrics, which can be utilized as optimization objectives in a performance-oriented architecture design. Generative adversarial networks (GANs) are generative models trained together with discriminative models as adversaries [24]. They generate images through implicitly high-dimensional distributions of data [25] that can be difficult to discern by humans. This can be applied to daylight prediction and a visual result generation that describe the daylight distribution in space, providing human designers with intuitive feedback and helping with design improvements [23].

Therefore, in this paper, a novel method is proposed for indoor daylight performance prediction based on CNNs and GANs for building design and optimization at the early design stage, when advanced computational simulation tools are challenged by complex input parameters and time and computation consumption, and proxy models based on machine learning are limited in terms of the building geometry. The proposed image-based models are more efficient with fewer unnecessary parameters than the simulation and can deal with a more general building geometry than proxy models.

## 1.2. Our study

To predict a daylight performance that can assist with the building design and support a performance optimization in form finding, we developed a surrogate model based on a deep learning method. Two datasets were constructed for a comparison and analysis of the model transfer. One is based on real cases of residential floorplans, whereas the other is generated automatically according to the control parameters. The CNN was trained on two datasets to predict the overall indicators, and the results were compared. Models were tested on the other dataset to analyze the transfer performance. The GAN was trained to predict the

illuminance values on the grids, and the results were visualized for intuitive feedback.

The remainder of this article is organized as follows: Section 2 provides a literature review of related studies conducted on daylight simulation proxy models based on machine learning methods and the application of deep learning methods in building performance research. Section 3 illustrates the network architectures of the CNN and GAN, construction of the two datasets and the complete workflow. Section 4 describes the analysis of the CNN prediction results on both datasets and displays the visual results of a GAN prediction. Section 5 discusses the possible application of the proposed model on design feedback as well as the limitations and expectations. Finally, Section 6 summarizes the main aspects of this article.

## 2. Related work

### 2.1. Daylight simulation proxy models based-on ML

Whereas advanced simulation tools are challenged by complex input parameters and time costs, proxy models have achieved success in the accurate prediction of specific situations and detailed annual image rendering. Neural networks and various traditional machine learning models have been adapted to the building of proxy models. In addition, artificial neural network (ANN) models have been trained to predict the illuminance on the work plane based on measured data to find the best position of the photosensor and daylight system control strategy [29]. ANNs have also been utilized to predict the illuminance for automated blind control optimization [30]. Moreover, fuzzy-inference systems (FIS) and ANNs have been trained on real measurement data to estimate the indoor illuminance at a particular spot in an office building [31,32]. Deep neural networks (DNNs) have also been trained based on simulated images for generating high-quality renderings of annual luminance maps from sun patch images and simulation parameters [33,34]. Traditional machine learning methods applied as daylight simulation proxies are summarized in Table 1. Different metrics of daylight performance provided by static and dynamic simulation calculations are set as target values to predict, and DA and sDA are the most widely used annual metrics. Climate-based daylight simulations depend on the specified location and corresponding weather file, based on which proxy models are developed for one or several specified cities. Although climate features have not been considered as input parameters yet, they have been learned and described as built-in model parameters. Therefore, different models need to be trained for different climates. Although proxy models based on machine learning have shown accurate predictions under certain circumstances, they have yet to be widely used as standard simulation tools.

The limitations of the proxy models mentioned above lie in datasets and building descriptions. During the training of proxy models, simulation results are considered as the ground truth in the training examples. Nevertheless, the datasets used for model training are commonly derived from parametric modeling, which cannot fully describe real room shapes [35–42]. Similarly, for input variables relevant to the building geometries, the building geometries are simplified and described based on room width, length, height, elevation, and window position, as listed in Table 1. The simplified parametric datasets and limited input variables of the proxy models hinder the transfer and reuse of the trained models in other projects. In addition, design and optimization based on proxy models are limited to fixed parameters and specific building forms. To adapt to various forms, shallow models require the development of high-dimensional geometric features and have become unable to be properly generalized [27,28]. This can be avoided by using a general-purpose deep learning procedure that can automatically learn good features. Therefore, in this study, CNNs and GANs are applied for general geometry feature extraction, and a dataset based on real cases is established to explore the differences.

**Table 1**

Studies on daylight simulation proxy modelNot clearly stated: MLR, multivariate linear regression; GP, Gaussian Processes; NB, Naïve Bayes; DT, Decision Tree; SVM, Support Vector Machine; FFN, feed-forward networks; RF, random forests; XGB, eXtreme Gradient Boosting Tree; SVR, Support Vector Regression; MLP, Multi-Layer Perceptron.

Year	Dataset	Case location	Input variables (geometry)	Model	Output metrics
2011 [36, 37]	Sensor data prototype	UCC, Ireland	Elevation, orientation, width, length, height, area, size, wall area, obstruction	NB, DT, SVM, regression	Illuminance class
2016 [35]	parametric	Izmir, Turkey	Orientation, room and window width, Length, height, window position	FFN, RF, SVM	illuminance DA, DGP
2017 [38]	parametric	Geneva, Switzerland	Building height, width, length, distance, depth	MLR and GP	sDA
2017 [39]	parametric	Berlin/Turin/Catania	Site, orientation, external obstructing angle, window size, room depth	Non-linear regression	DA, DA <sub>con</sub> , sDA
2018 [40]	parametric	Fixed	Window dimension, location	ANN	DA
2019 [41]	Parametric	Fixed	Window width, height, WWR, sill height	MLR	sDA, ASE, TECL, TECC, TEC
2020 [42]	parametric	Harbin, China	Width, depth, height, sill height, WWR, WSR, orientation	XGB, RF, SVR, MLP	UDI

## 2.2. Application of CV and DL in building performance

CV methods have recently achieved success in building occupancy detection and prediction related to image/video processing [43–45]. Images and videos from the camera and different sensors were analyzed by various CV algorithms. A novel sensor based on long-wave infra-red (LWIR) collects thermal images, which are then analyzed using Kalman filtering, region growing and blob detection [46]. A pan-tilt-zoom (PTZ) camera and overhead video are used for face recognition and people counting in a lecture room with up to 200 people combined with CO<sub>2</sub> sensors [47]. Depth images recorded by a Kinect camera have been analyzed using the waterfilling algorithm, Munkres assignment algorithm, and SVM [48,49]. HOG-SVM, CNN and K-means have also been utilized to analyze office surveillance videos in Ref. [50]. A GAN has been used to handle complex occupancy modeling without specific assumptions [52]. CNN-based models have been developed to detect and classify occupancy activities and estimate personnel occupancy loads to optimize the system control [53,54].

In addition to occupancy photo detection, DL methods have been applied to a variety of images to solve tasks relevant to building performance, and this section focuses on the use of CNNs and GANs. CNNs are used in the detection of building materials and types of lateral-load resisting systems for cost-effective exposure models on the street level in urban photos [55]. They are also utilized in the modeling of legibility in indoor spaces and the spatial and visual connectivity of workplace layouts [56,57]. A new image-based indoor localization method using building information modeling (BIM) and CNNs was proposed to identify the location and orientation of mobile device users [58]. Voltage-current (VI) trajectories are represented as weighted pixelated images and CNNs automatically extract relevant spatial features [59]. Variational autoencoders (VAE) coupled with convolutional layers (VAE-CNN) were conducted to avoid data missing in the indoor air quality (IAQ) system [60].

CNNs and GANs can handle more data formats than images in building performance research and are widely used to extract complex features and generate samples. A half-hourly time-step predictive model integrating a CNN with a long short-term memory network (LSTM) is proposed for solar radiation [61]. A novel deep learning network, i.e. an autoencoder long-term recurrent convolutional network, was developed to distinguish common human activities using commodity WiFi-enabled IoT devices [62]. GANs are utilized to address the imbalanced data problem and are integrated with base classifiers for fault detection and diagnosis (FDD) [63,64]. They are also applied to generate building electrical load profiles that can capture the stochastic variations of actual buildings [65]. A CNN and seq2seq were built as metamodels to predict the hygrothermal time series of building components and energy consumption transfer learning [66,67]. A CNN-based surrogate computational fluid dynamics (CFD) model was also proposed to

efficiently approximate solutions for non-uniform steady laminar flows [68]. As for urban airflow, autoencoders with CNN (AE-CNN) are constructed [69]. A GAN has been used for annual daylight metric prediction based on input images of doors, windows and walls. The outputs are images generated by a GAN and are visually similar to the simulation results, despite a lack of quantitative metrics [70]. In our study, a CNN is conducted to predict quantitative daylight metrics as a supplement to the visual prediction of a GAN, and an image encoding method considering the distance information is proposed.

## 3. Methods

The workflow of CNNs and GANs trained as proxy models for daylight prediction is illustrated in Fig. 1. The datasets provide basic geometry information of floorplans or rooms, according to which 3D geometry models are rebuilt in SketchUp and Rhino with Grasshopper (GH) and grids are generated for simulation through MOOSAS or GH. The results of the simulation calculation by RAIDIANC and DAYSIM (Honeybee) are encoded as images, and the overall metrics are calculated, which serve as the outputs of the GAN and CNN, respectively. For the input of the networks, the geometry data of the samples are encoded as images. After model training, proxy models can predict the daylight performance of new cases. Network architectures and the basic theory of CNNs and GANs are introduced in Section 3.1. Details about the dataset construction and processing of the simulation results are illustrated in Section 3.2 and Section 3.3.

### 3.1. Network architecture

#### 3.1.1. ResNet, a CNN architecture

ResNet is a residual learning framework proposed to address the degradation problem and make deep networks easier to optimize [71, 72]. An excellent performance in image classification, detection and segmentation competitions has proven the accuracy of the method. With the ability to extract different levels of features from image, ResNet is trained for overall daylight metric prediction.

Considering the training time and accuracy, ResNet50 is adopted in this study, and is composed of 3-layer bottleneck building blocks, as illustrated in Fig. 2. Grayscale images encoded with the building geometry information, as illustrated in Section 3.2.3, are inputs of the first convolutional layer followed by 16 building bottleneck blocks with different numbers of filters. A bottleneck block is a stack of three layers of convolution for the residual function. In residual learning, a residual function  $F(x) := H(x) - x$  is explicitly approximated, where  $x$  denotes the inputs. Thus the underlying mapping function  $H(x)$  becomes  $F(x) + x$ , and the operation is performed by a shortcut connection and element-wise addition. The parameter-free identity shortcuts lead to efficient models with high accuracy. To predict the values of the three static and

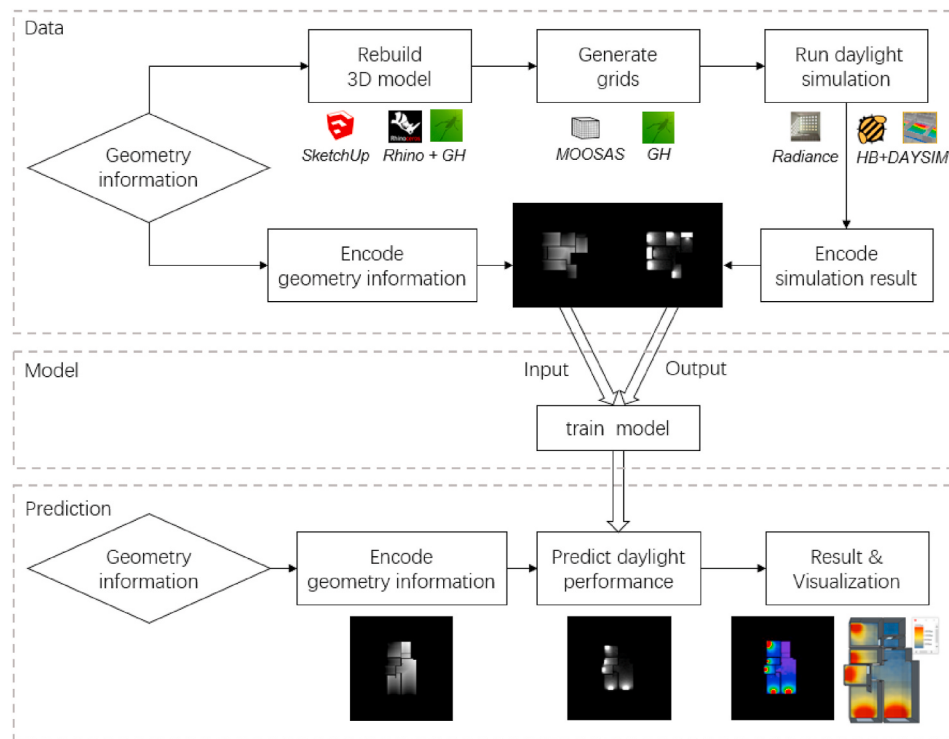


**Fig. 1.** Workflow of training and prediction of proxy model.

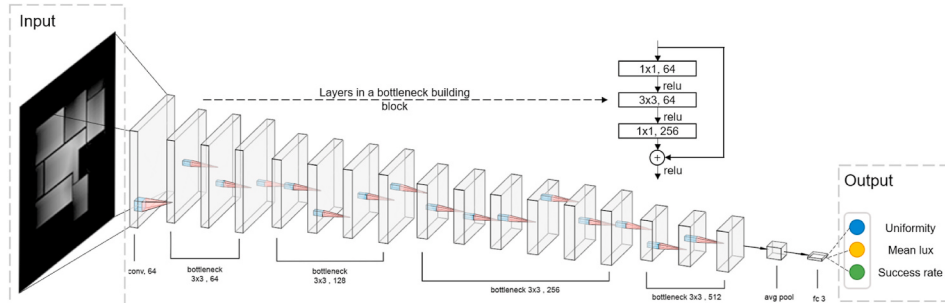


**Fig. 2.** The architecture of ResNet50 network.

two annual daylight performance metrics defined in Section 3.3, ResNet50, originally used for classification, was adapted to solve the regression problem. Taking the static metric prediction as an example, the dimension of the output layer is set to 3, and tanh is used as the activation function for the dense layer. The mean squared error (MSE) is taken as the loss function for the training. The daylight uniformity, mean lux, and success rate were predicted as outputs. For annual metrics, only the number of outputs is changed.

### 3.1.2. Pix2pix, the GAN architecture

Pix2pix is a common framework for image-to-image translation problems based on conditional GANs (CGAN) and has achieved success in synthesizing photos from label maps, coloring images and other image translation tasks [73]. Predicting the illuminance values according to geometric information can also be considered as a translation task. Therefore, we used pix2pix to predict grid-based illuminance as a metamodel.

GANs train a discriminator to distinguish between real and generated images while simultaneously training a generative model. As a conditional GAN, the discriminator of pix2pix makes a decision based on a pair of images, and both the generated and original inputs considered, as shown in Fig. 3. The generator also learns to generate from the input

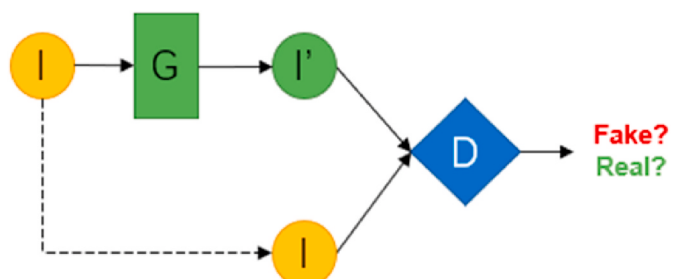


**Fig. 3.** The concept of CGAN.

image and fool the discriminator.

The architecture of the pix2pix network used in this study is illustrated in Fig. 4. The generator was adapted from U-Net [74] with skip connections between the mirrored layers. Inputs are grayscale images of the floorplans, whereas the geometry information of the space partitions and windows are encoded using the distance. Based on the encoded images, the generator learns to predict and fool the discriminator. Truth images are encoded with the simulation results, where each pixel

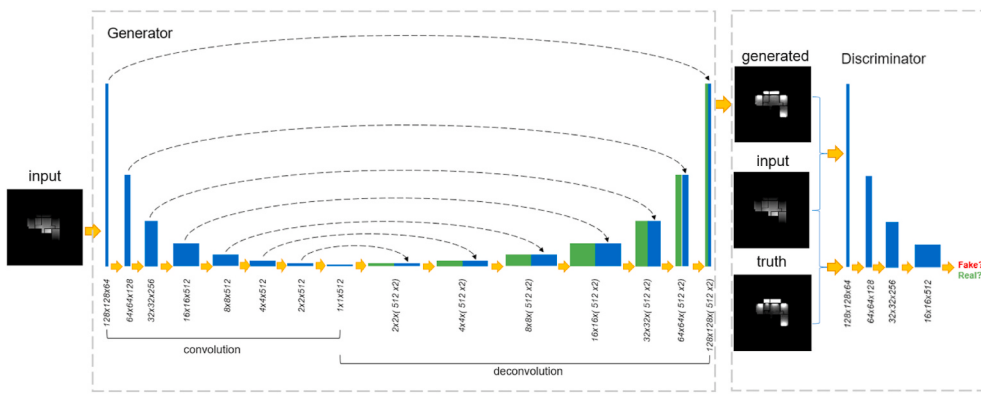


Fig. 4. The architecture of pix2pix network.

represents a grid within the space, and the discriminator learns from pairs of images, which are original inputs combined with the generated images (fake) or ground truth (real). The cross entropy loss is calculated as the discriminator loss, and the L1 term is included in the generator loss. The trained generator can generate images for the prediction of the illuminance as a proxy model.

### 3.2. Datasets

Two different datasets are established in this study. One is based on real residential floorplans, whereas the other is based on parametric modeling, similar to previous studies on proxy models. The datasets were used for model training, and the results were compared. The models were also tested on each other to explore the possibility of a model transfer. In addition, the method of image encoding is described in this section.

#### 3.2.1. Parametric box dataset

The parametric box dataset is composed of simple shoe-box rooms generated automatically according to parameters including room width, room depth, window-to-wall ratio (WWR), and window orientation, as listed in Table 2. By combining the parameters, 600 examples were generated, as shown in Fig. 5, and 575 of them were selected to construct the dataset to keep the same data volume as the real-case dataset.

#### 3.2.2. Real-case dataset

Data for the real-case dataset were collected from automatic recognition results of real residential floorplans in Beijing, which contain more complicated and irregular indoor partitions. The geometry information of the rooms and openings, including windows and doors, are used. The shapes of rooms are denoted with an ordered list of vertexes, and every opening is denoted by a pair of endpoints, which contain information on the locations and dimensions of the building components in complex real floorplans.

To enlarge the dataset and reduce an overfitting, cases are transformed to generate new floorplans for data augmentation, which is an easy and commonly used method in machine learning. Real-case data were augmented by changing the room depth and window width. The depths of the rooms facing south and north are increased by 0.6, 1.0, 1.6 and 2 m, and the widths of the windows are reduced by 20%, 30%, 40%,

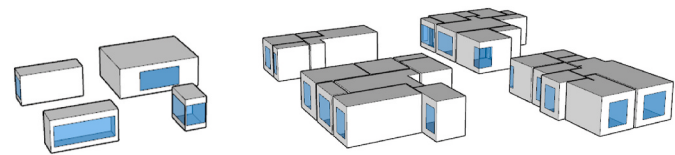


Fig. 5. Several examples in two datasets: left, parametric box; right, real case.

and 50%, respectively. The augmented examples are labeled automatically through a simulation calculation and incur no additional labor cost. Real-case dataset contains 575 examples in total, as shown in Fig. 5.

#### 3.2.3. Image encoding

Geometry data are encoded as grayscale images and input into ResNet and pix2pix, as shown in Fig. 6(a). Considering that the room shape and indoor partitions have a significant influence on the indoor daylight performance, the distance to the window is taken into consideration.

To encode the geometric information into images, a pre-processing procedure is needed to obtain the basic geometric information of walls, doors and windows. The specific parameters of the three types of objects are shown in Fig. 6(b). A room is described by a list of points in order; thus, the space can be enclosed by connecting the points sequentially. Each point is denoted by (x, y). Nonrectangular rooms with multiple linear boundaries can be denoted as room 5, but curved walls are beyond the scope of this study. A window is part of a room boundary connecting the indoor and outdoor spaces. Therefore, windows have no thickness in the model and are denoted as a pair of vertices (x<sub>1</sub>, y<sub>1</sub>) and (x<sub>2</sub>, y<sub>2</sub>). A door connects the boundaries of two rooms and is described as a rectangle in the floorplan. Therefore, a door can be denoted by four points that enclose an area. Walls are not considered particularly as objects in this study, and gaps between adjacent rooms are internal walls. The thickness of the external walls is ignored.

Such geometric information can be easily extracted from various design models, such as DWG, DXF, and PDF, etc. This study focuses on the information encoding method by introducing the distance to the window into the input image, and a building model format transfer is out of the scope of this research. In this study, parameters are derived from the recognition results of floorplan images for the real-case dataset, whereas for the parametric generated dataset, parameters are directly obtained from the design parameters in Table 2.

The calculation method for the brightness value of each pixel is illustrated in Fig. 6(b). In the encoded images, coordinates in meters are rounded to 0.1 and mapped to the pixel positions. Every pixel corresponds to a grid in a daylight simulation with a size of 0.1 m × 0.1 m, and the brightness values of the pixels represent the Manhattan Distance to the nearest window, which indicates the influence of the room shape

Table 2

Parametric box dataset generation parameters.

Parameters	Values
Room width	2, 4, 6, 8, 10 m
Room depth	2, 3, 4, 5, 6 m
WWR	0.9, 0.7, 0.5, 0.3
Window orientation	S, N, W, E, S + W, S + E

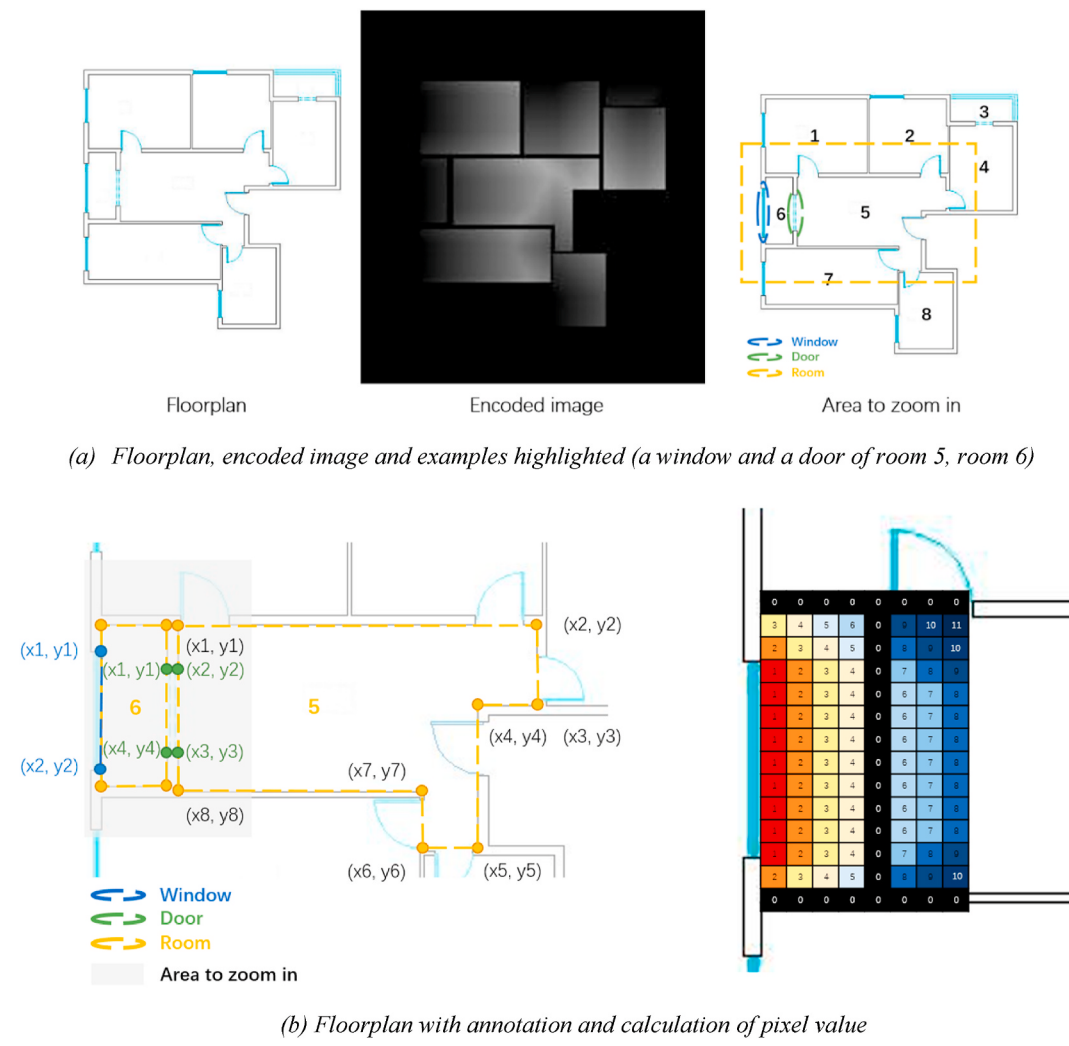


**Fig. 6.** Illustration of the image encoding method.

and indoor partitions. Areas that are not covered by simulation grids, including walls, openings, and outdoor areas, were set to zero. Only some of the grids are displayed and the grid size is enlarged simply to show the process clearly. However, 0.1 m is used in reality, and the false color is applied to show the greyscale images better and has no influence on the encoded results.

### 3.3. Daylight simulation

The results of the daylight simulation are considered as the ground truth in model training. Simulations of the two datasets were conducted based on RADIANCE/DAYSIM, which are validated simulation engines for daylighting that are widely used by simulation tools including DIVA, honeybee and Design Builder. To automatically conduct simulations on the datasets, 3D models were rebuilt according to geometry data in SketchUp/Rhino with GH. For the two datasets, geometry data only comprise 2D information of the layouts without vertical information such as room height, window sill and window height. Therefore, the parameters are set to the same default values. Consequently, evaluations and predictions merely reflect the influence of the floorplans on the daylight performance, and facades are not considered. For the rebuilt geometry models, MOOSAS [7]/GH automatically generates grids for each indoor room and calls RADIANCE/DAYSIM for the simulation calculations. The important simulation parameters and default height parameters are listed in Table 3. Followed the design drawings, encoded images take the upward direction as the north as well.

**Table 3**  
Simulation parameters.

Parameter	Value
Room height	3 m
Window sill	0.5 m
Window height	1.9 m
Door height	2.2 m
Ambient bounces(ab)	4
Ambient division(ad)	256
Ambient accuracy(aa)	0.15
Sky	Uniform cloudy sky
Time	Mar 22nd 14:00
Site location (latitude, longitude)	39.92, 116.46

For the simulation results, horizontal illuminance is the most widely applied architectural lighting design metric for judging whether daylighting is sufficient, thus further influencing the energy use and level of comfort [77]. Based on the illuminance, the daylight factor (DF) and annual daylight metrics, such as daylight autonomy (DA) and useful daylight illuminances (UDI), have been developed.

In this study, illuminance values in lux are mapped to grayscale images as outputs of pix2pix. The locations of the grid can be found in the encoded images. ResNets are trained to predict both static and annual daylight metrics. For static daylight performance, three typical integral metrics were derived from the illuminance values, including uniformity, mean lux, and success ratio. The daylight uniformity is a

commonly used illuminance metric that measures daylight distribution on the reference plane with a single value and is defined as  $\text{min}(\text{illuminance})/\text{mean}(\text{illuminance})$ . The mean lux is the average illuminance value in lux and reflects the overall daylight performance. The success rate is the percentage of grids that exceed 300 lx, which measures in how much area the required illuminance level is achieved. The three illuminance-based daylight metrics describe the different features of daylight quality. For annual daylight performance, sDA (spatial Daylight Autonomy) and UDI>50 are two typical integral metrics derived from DA and UDI. DA and UDI measure the percentage of the occupied times of the year when the minimum illuminance (300 lux) can be maintained, and illuminances within a range of 100–2000 lux are achieved [78,79]. Named by IES, sDA measures the percentage of the analysis area where  $\text{DA}_{300} > 50\%$ . Similarly, UDI>50 measures the percentage of the analysis area where  $\text{UDI}_{100-2000} > 50\%$ . In addition to the three static metrics and two annual metrics described above, the proposed prediction method can also be applied to other metrics.

## 4. Results

### 4.1. CNN prediction of daylight metrics

For the three static daylight metrics, i.e., mean lux, uniformity and success rate, ResNet50 was trained and tested on both the real-case dataset and the parametric box dataset. Both datasets were divided into training set of 70%, validation set of 15%, and test set of 15%. The accuracy curves of the training and validation set illustrate the process of model convergence, as shown in Fig. 7. The models of the two datasets underwent a similar process in that the validation error began to be lower than training error and then increased to close to the initial training error, finally decreasing to slightly higher than the training error. Both models converged to a relatively low and stable error rate after 200 epochs.

The two datasets have different sampling and margin probabilities in the feature domain, which may further influence model prediction and transfer performance. Although the distributions of the input geometry are difficult to quantify and visualize, the distributions of the three metrics may also reflect the differences. As shown in Fig. 8, the success rate of the real-case dataset is more scattered, whereas the uniformity and mean lux are more centered. By contrast, the success rate of the parametric box dataset is more centered whereas the uniformity and mean lux are more scattered. The parametric box dataset shows higher values for all metrics because there is no partition in the simplified box room.

To measure the prediction performance of the two models, the coefficient of determination ( $R^2$ ) and mean square error (MSE) were calculated in (1)–(4). The coefficient of determination quantifies the degree of linear correlation between the prediction and truth by calculating the accounted percentage. An  $R^2$  value close to 1 indicates high

goodness of fit. The MSE measures the difference between the predicted and true values. An MSE close to zero indicates a small error and high accuracy.

$$\text{SSE} \cdot = \sum_i (y_i - \hat{y}_i)^2 \quad (1)$$

$$\text{SST} \cdot = \sum_i (y_i - \bar{y})^2 \quad (2)$$

$$R^2 \cdot = 1 - \frac{\text{SSE} \cdot}{\text{SST} \cdot} \quad (3)$$

$$MSE \cdot = \frac{1}{n} \sum_{i=1}^n (\hat{y}_i - y_i)^2 \quad (4)$$

The prediction performance on three daylight metrics including daylight uniformity, mean lux and success rate is listed in Table 4. The two models trained on the real-case dataset and parametric box dataset were compared in both the training and test sets.

For the prediction of daylight uniformity,  $R^2$  of the real case dataset was larger than that of the parametric box dataset in both the training and test sets, which indicates better fitness. In addition, the MSE is smaller, which indicates a higher accuracy. The prediction results for the standardized daylight uniformity metric are displayed in Fig. 9. Both the training and test samples in the real case dataset are more concentrated, whereas those in the parametric box dataset are scattered. The difference in distribution can explain the different fitness levels of the two models.

For the prediction of the mean lux,  $R^2$  in the training set of the two models is close, and the parametric box dataset maintains a similar performance in the test set, whereas the real-case dataset performs worse in the test set. Although the real-case dataset achieved a lower MSE than the parametric box dataset in the training set, they were close in the test set. The predictions of the standardized mean lux are shown in Fig. 10. The different performances of the parametric box dataset model on the training and test sets indicate a slight overfit or sample randomness.

For predicting the success rate, the  $R^2$  values of both the real-case dataset and parametric box datasets are close, whereas the MSE of the real-case dataset was smaller for both the training and test sets. In the parametric box dataset, as shown in Fig. 11, a cluster of points is concentrated at near (1, 1), which represents a room with a relatively small depth and a large WWR, where the illuminance of nearly all grids is above 300 lx. Nevertheless, this is not common in real cases and indicates a biased distribution of the parametric box dataset.

Another ResNet50 model is trained for a prediction of the annual daylight metrics, including sDA and UDI >50. The model is trained on the real-case dataset, and its prediction performance is displayed in Table 5.

For both sDA and UDI>50,  $R^2$  is higher on the training set but lower

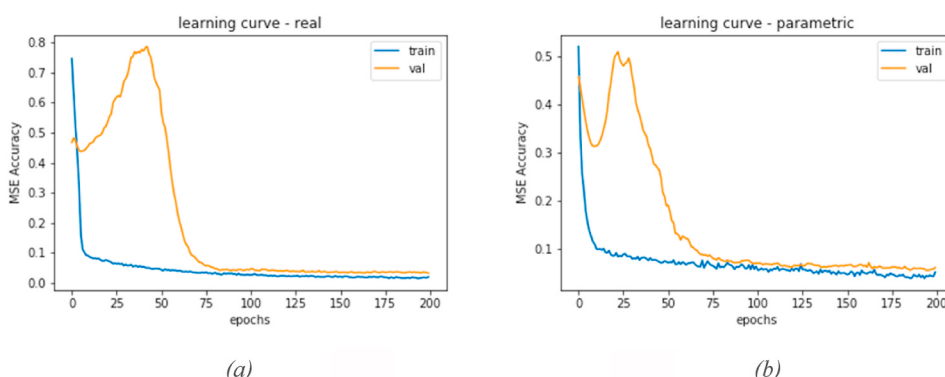


**Fig. 7.** Learning curves of (a) real-case dataset and (b) parametric box dataset.

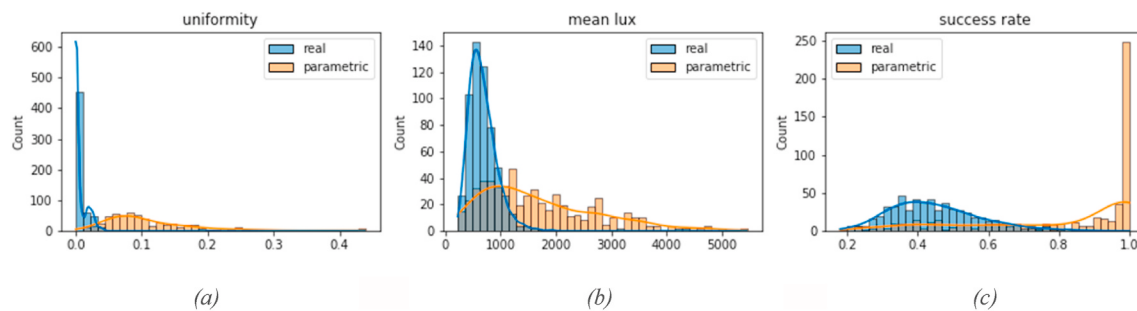


**Fig. 8.** Distribution of metrics on two datasets including (a) uniformity, (b) mean lux, and (c) success rate.

**Table 4**  
Prediction accuracy of ResNet50 on two datasets.

Daylight	Dataset	R <sup>2</sup>		MSE	
		training	test	training	test
Uniformity	Real case	<b>0.965</b>	<b>0.959</b>	<b>0.006</b>	<b>0.008</b>
	Parametric box	0.689	0.638	0.040	0.073
Mean lux	Real case	0.867	0.629	<b>0.010</b>	0.036
	Parametric box	0.871	<b>0.814</b>	0.020	0.038
Success rate	Real case	0.892	0.733	<b>0.012</b>	<b>0.039</b>
	Parametric box	0.901	0.812	0.034	0.074

on the test set, and the MSE is lower on the training set, which indicates that the model tends to overfit. In the real-case dataset, the distributions of sDA and UDI are scattered, as shown in Fig. 12. Annual daylight metric prediction is a more complicated task than static daylight. Thus, larger datasets are needed to train a more general model and improve the prediction performance.

To evaluate the possibility of a model transfer and apply the trained model on different datasets, a model trained on the real-case dataset (M1) was tested on the parametric box dataset (T2) and vice versa. The two models aim to solve the same task, but learn from different domains with different features and distributions. The prediction performance of the transferred models is compared with previous results in Section 4.1, as shown in Table 6.

As the transfer prediction task, the  $R^2$  values of M2T1 and M1T2 are far from 1 or even negative, which illustrates the poor fitness on different datasets. Some dimensions and sizes in the parametric box dataset are not realistic and may not occur in real cases, whereas the real-case dataset only represents certain residential floorplans in Beijing. Neither of the two datasets are sufficiently large or well-annotated to be

used for model pre-training, and the prediction accuracy needs to be further improved. Therefore, larger datasets that cover a greater probability and are properly sampled are a direction for future study. This also reveals a common problem for the black-box model developed for specific problems. Unlike shallow machine learning models that already have features selected based on professional knowledge, statistical methods, or feature importance, deep learning methods learn the feature extraction from the data. This allows a relatively free format of input owing to a high dimensionality and contains the potential for transfer learning, which means that knowledge of some previous tasks can be transferred to different domains or different tasks [75].

#### 4.2. GAN prediction of visual result

Pix2pix is trained on the real-case dataset to generate images of the predicted illuminance. The dataset was divided into a training set of 70%, validation set of 15% and test set of 15%. The discriminator and generator both converged after 200 epochs, as indicated by the learning curves in Fig. 13.

To visualize the learning process of the generator, images generated in different epochs are logged and plotted in Fig. 14. First, the edges are blurred, and local periodic textures appear when the network parameters are not fully optimized with a high training error. From epochs 10 through 80, the edges become clearer, and the textures that are inconsistent with the input disappear gradually as the training error decreases and the model converges. Images after 80 epochs remain almost unchanged and look similar as the training error becomes more stable and smaller in size.

The prediction results are close to the ground truth simulation results in visualization and are able to provide effective feedback on the daylight performance at the early design stage. Pixels in the output

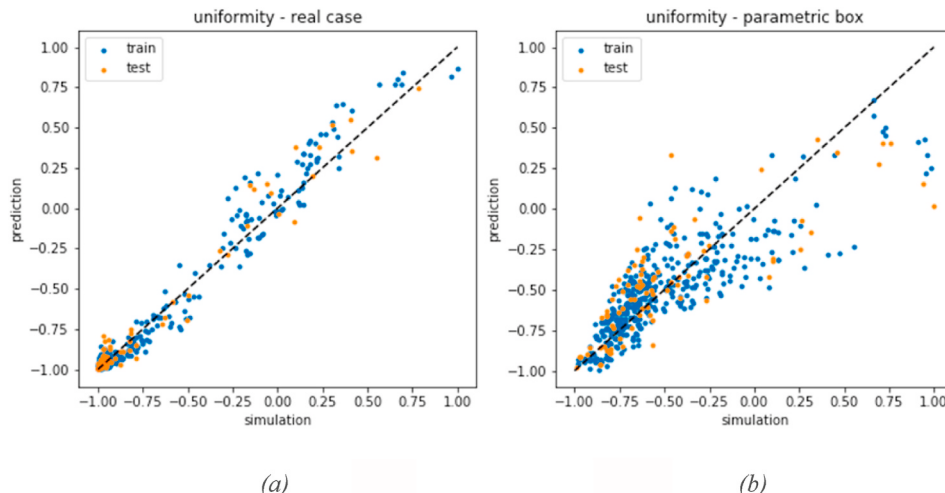


**Fig. 9.** Prediction of daylight uniformity on training and test sets of (a) real-case dataset, and (b) parametric box dataset.

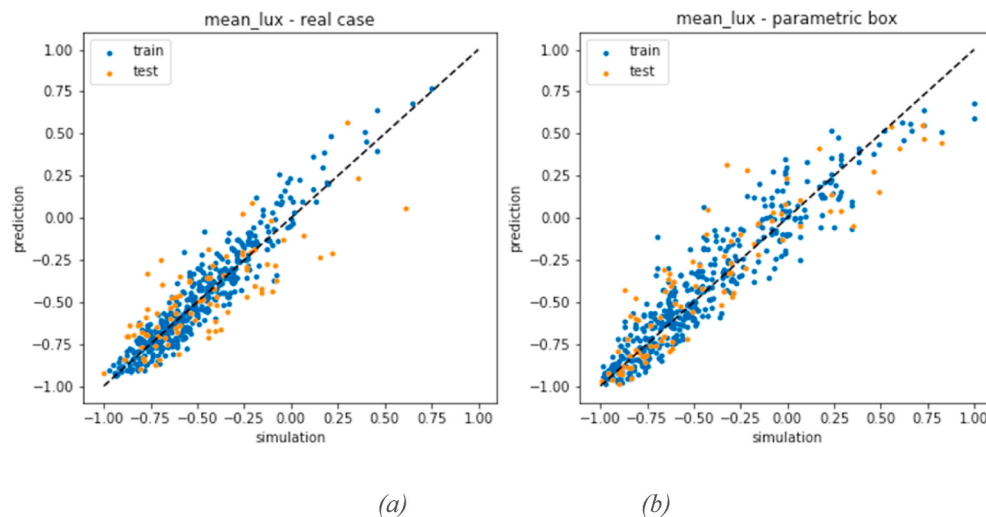


**Fig. 10.** Prediction of mean lux on training and test sets of (a) real-case dataset, and (b) parametric box dataset.

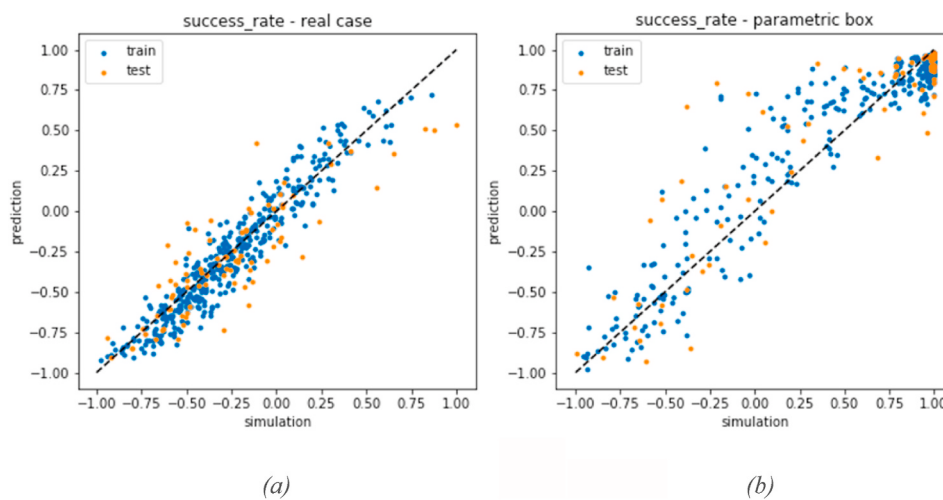


**Fig. 11.** Prediction of success rate on training and test set of (a) real-case dataset, and (b) parametric box dataset.

**Table 5**  
Prediction accuracy of ResNet50 on annual daylight metrics.

Daylight metric	Dataset	R <sup>2</sup>	MSE
sDA	Training	<b>0.886</b>	<b>0.020</b>
	test	0.650	0.076
UDI>50	training	0.846	0.021
	test	0.608	0.061

image denote grids in the grid-based illuminance simulation, and the images are mapped to false colors, as shown in Fig. 15. In images of errors, the pixel colors are errors in RGB values between the prediction and ground truth images reporting a color deviation, instead of the illuminance values, where dark areas are the same in the ground truth and prediction.

To quantitatively evaluate the image quality generated by the GAN in this study, the structural similarity (SSIM) index is selected. Whereas other quality metrics such as the mean squared error (MSE) and peak signal-to-noise ratio (PSNR) do not match the perceived visual quality, SSIM is a widely used objective image quality assessment based on the hypothesis that the human visual system (HVS) is highly adapted for structural information [76]. The SSIM value is generally no larger than 1, and when it equals 1, it indicates that the two images are exactly the

same. For the test set, the simulation and predicted results were measured, and the mean value of SSIM was 0.90.

Images generated by the model can be transferred into the illuminance value and rendered in the design model as surrogates of the simulation results, as shown in Fig. 16. A visualization of the illuminance values offers intuitive feedback for human designers of the overall situation and daylight distribution within the space, allowing designers to decide how to improve the areas experiencing a poor performance. Under such circumstance, the balance of accuracy and computational cost is achieved using the proxy model based on a GAN, which fulfills the requirement of real-time feedback in the early design stage.

## 5. Discussions

The proposed metamodel can provide real-time feedback for the early design stage with both quantitative and visual results of indoor daylight performance. For an automatic multi-objective optimization workflow, static daylight metrics, i.e., the mean lux, uniformity, and success rate, and annual metrics, i.e., sDA and UDI >50, can be quickly predicted as part of the objectives. The time cost in each iteration is significantly reduced, and the exploration of a wider design space can be more efficient. For human designers, daylight metrics can be compared with design standards or targets, and the floorplan can be adjusted with

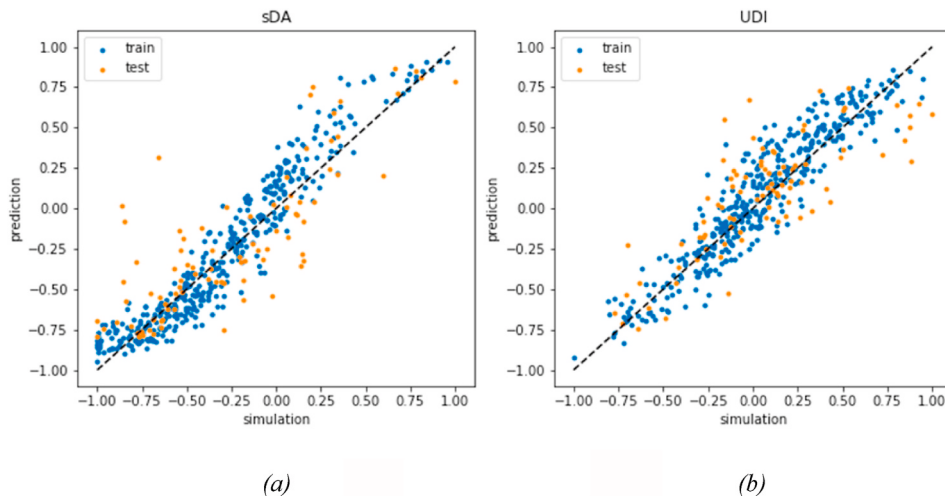


**Fig. 12.** Prediction of (a) sDA, and (b) UDI on training and test set.

**Table 6**  
Transfer performance of ResNet50 for daylight prediction.

Daylight metric	Accuracy metric	M1T1	M2T1	M1T2	M2T2
Uniformity	R <sup>2</sup>	<b>0.959</b>	0.048	-0.560	0.638
	MSE	<b>0.008</b>	0.187	0.315	0.073
Mean lux	R <sup>2</sup>	0.629	-1.915	0.091	<b>0.814</b>
	MSE	<b>0.036</b>	0.285	0.185	<b>0.038</b>
Success rate	R <sup>2</sup>	<b>0.733</b>	-0.955	0.609	<b>0.812</b>
	MSE	<b>0.039</b>	0.284	0.154	0.074

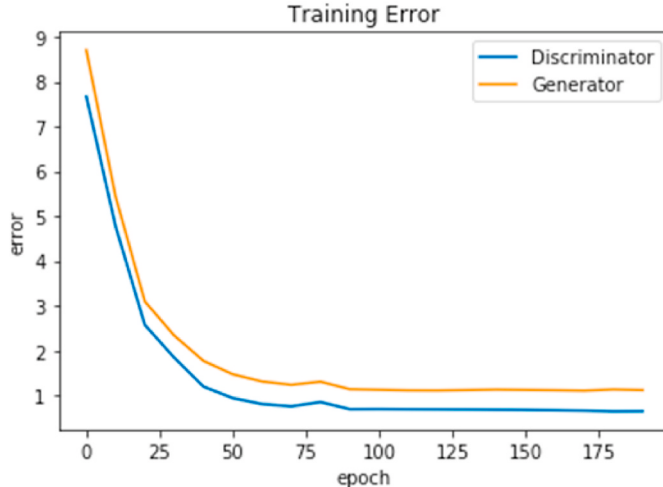


**Fig. 13.** The learning curve of pix2pix.

reference to the visual results. For instance, if the mean illuminance and success rate are both low, more glazing areas can be added. If the mean illuminance is fine but the uniformity is low, designers can investigate the visualization result to locate the worst area and adjust the partitions or windows to improve it. If the mean illuminance is high but the uniformity is low, smaller windows or shading can be considered. An accurate simulation with more complex parameters can be conducted in a more detailed later design stage. Daylight is one of the many performances to optimize in a design process, and the quick quantitative feedback can provide objective reference for weighing against other factors and decision making.

The time costs of the proposed prediction models are compared with

the simulation tools. Test is run on a computer with Intel(R) Core (TM) i7-7700HQ CPU @ 2.80 GHz and memory of 16 GB. For the CNN and GAN, the time cost of model loading, pre-processing, and prediction are evaluated and compared. Notably, models only need to be loaded once and can predict different designs iteratively. The pre-processing, namely image encoding, are the same for CNN and GAN, and the average time cost on our dataset is 0.3s including geometry file loading, distance calculation and image saving. For the simulation tools, pre-processing, including a grid generation and simulation parameter configuration, is relatively fast, and thus only the most time-consuming process, i.e., the simulation calculation, is counted. Radiance and DAYSIM are both validated and widely used simulation tools, so their speeds are tested as benchmark. ClimateStudio is also tested as a state-of-the-art and fastest simulation software that implements Radiance in a progressive path tracing mode [80].

As listed in Table 7, once loaded, the proposed metamodels can predict static or annual results in 0.4–0.55s. For static simulation, time costs of Radiance are among 5–10s. For annual simulation, time costs of DAYSIM and ClimateStudio are 3–5 min and 15–40 s, respectively. The time costs of ClimateStudio are influenced by the number of sensors and model complexity, and the simulations can be stopped during the progressive process, so the time cost differs when stopped after different passes. The fastest result can be generated just after the first pass. For the smallest model with an area of 30 m<sup>2</sup> and 1681 sensors (2630 grids in the proposed method), time costs are 12 s for initialization and 3 s for every pass. For the largest model with an area of 90 m<sup>2</sup> and 5945 sensors (8732 grids in the proposed method), time costs are 29 s for initialization and 11 s for every pass. The simulation tools have the advantages that useful intermediate results are saved like illuminance of every hour, which is not quite necessary in early design stage, but are meaningful for detailed design optimization like material property.

The speeds of the proposed prediction models are also compared with traditional simulation methods after acceleration. Considering the speed, accuracy and limitations, the simulations and proxy models complement each other and are suitable for different design stages. The proposed proxy models can respond within 1s once loaded and are more suitable for the automated optimization at early design stage when design details are hard to be specified and the potential for a performance improvement lies on the building form and indoor partition. On the contrary, physical-based calculation methods like ray tracing and radiosity are more reliable and compatible with various building situations, and are more suitable for accurate evaluation in the subsequent detailed design stages. However, the detailed parameter setting and computation complexity can hinder annual daylight simulations from automated optimization at early design stage. Efforts were made to

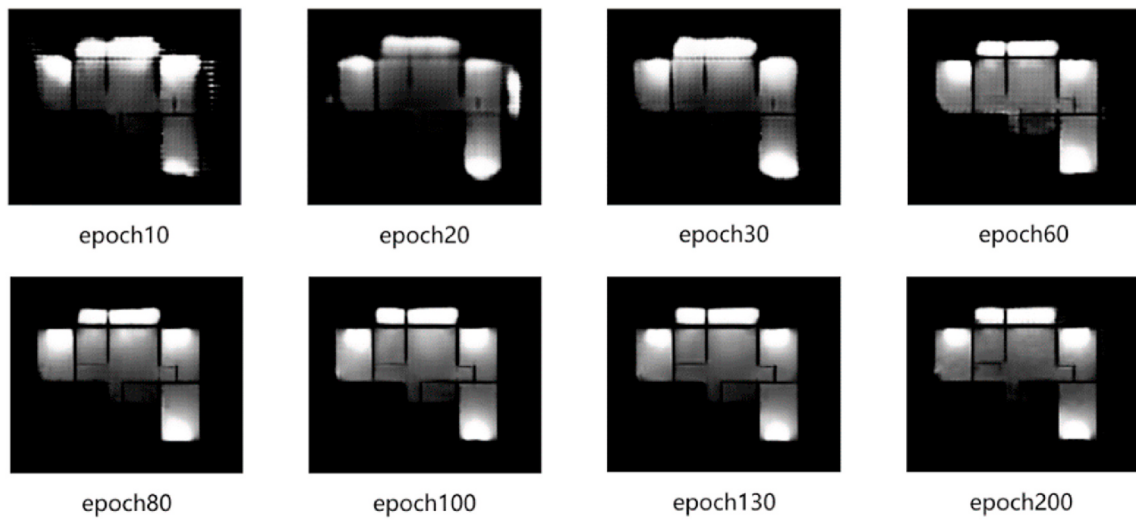


Fig. 14. The learning process.

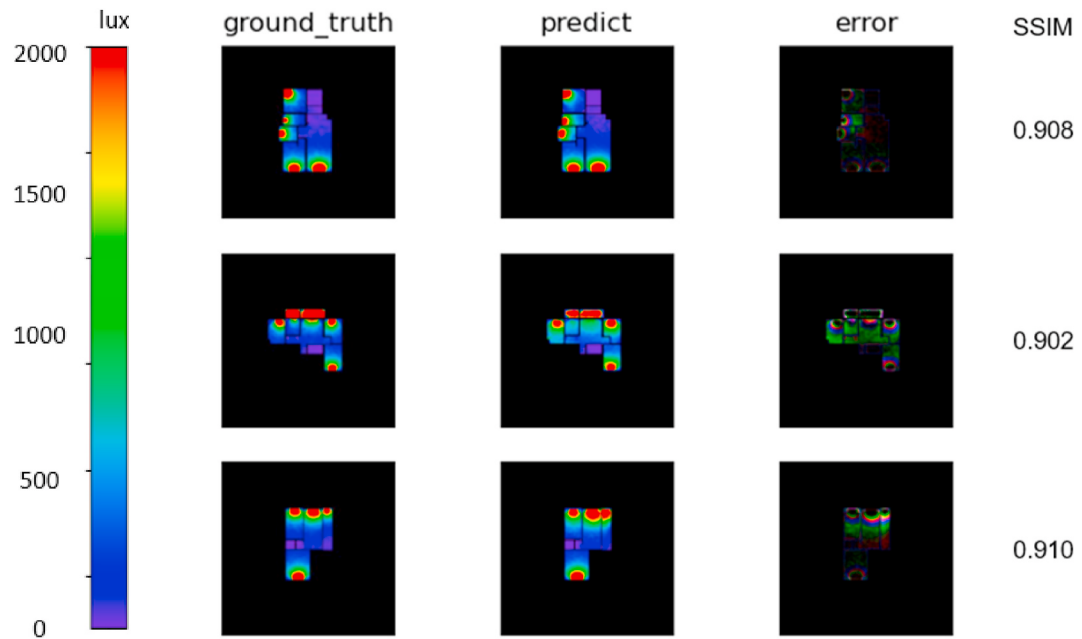


Fig. 15. The illuminance prediction for three cases.

speed up the simulation methods including hardware acceleration and algorithm simplification. For hardware acceleration, Radiance 3–5 phase simulations were accelerated through parallel calculation based on Graphics Processing Units (GPUs), and the matrix operations can be accelerated up to 100 times [11,12], while the whole simulation can be 25 times faster [13]. For the small and large model with 2850 and 14250 sensors, best time costs were 2.6 and 22.2 min, respectively [13], while the proposed model can handle up to 8732 sensors in 0.4s. Through algorithm simplification and reduction of the number of sensors/test points, the improved method can be up to 84 times faster than the standard DAYSIM/Radiance approach [14], while our method is 450–750 times faster than DAYSIM without loss of test points.

Three static and two annual daylight metrics based on illuminance were predicted, and the feasibility of applying CNNs for daylight prediction tasks was proved. However, the prediction of static daylight metrics is more accurate than that of annual daylight metrics on the same dataset and model. Annual daylight metrics consider climate change over the entire year and contain more complicated features.

Thus, a larger dataset should be used, and the model should be optimized to achieve a better prediction. The ability of GANs to predict the illuminance was also verified, although only the illuminance values at a specific time based on a static daylight simulation were applied. For annual daylight metrics such as DA and ASE using a grid, the workflow is exactly the same, but larger datasets are required.

Besides the advantages of the proposed method mentioned above, there are some limitations to this study, which can be addressed in future research. In this research, the models were trained using the climate file specified for Beijing, China, and cannot be used for predictions in other locations. For different climates, models need to be trained separately or transferred by introducing new climate features. For the building orientation, cases in the two datasets are in the south-north direction and divided into orthogonal grids. Thus, the prediction of rotated buildings requires further training with augmented datasets. The grid size is fixed to 0.1 m at present, and future work should explore different scales to cover various floor areas. For floorplans in larger areas such as office buildings, a larger grid size, including 0.5 m × 0.5 m can

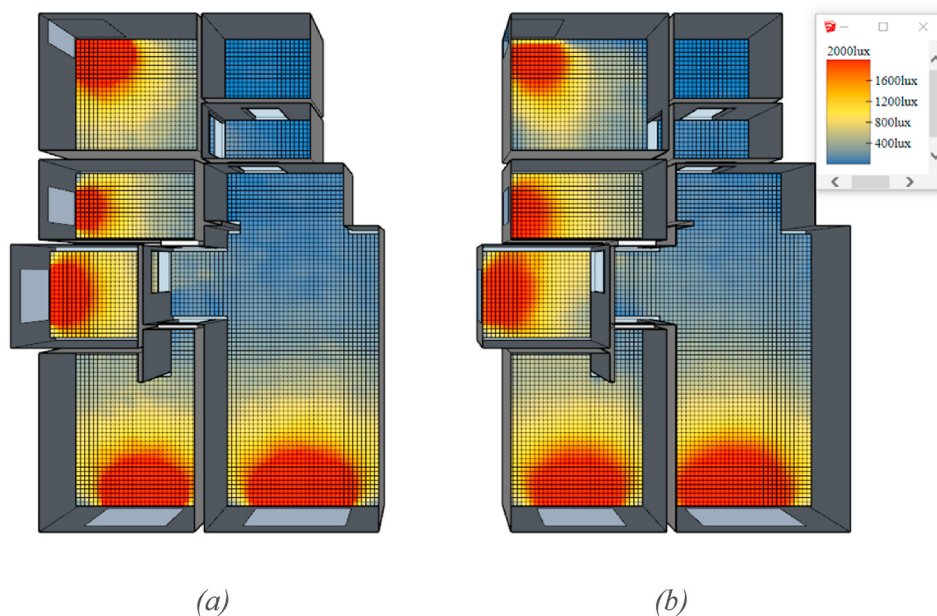


**Fig. 16.** The prediction results in SketchUp model by (a) simulation, and (b) the proposed prediction model.

**Table 7**  
Time cost of proxy model VS simulation calculation.

	metrics	Static			Annual		
		load	pre-process	predict	load	pre-process	predict
Metamodels	CNN	2.5s	0.3s	0.1s	2.5s	0.3s	0.1s
	GAN	0.6s	0.3s	0.25s	-	-	-
Simulation tools	Radiance	5–10s					
	DAYSIM	-					3–5min
	ClimateStudio	-			initialization 12–29s		every pass 3–11s

be set to a single pixel. In addition, the heights of the windows and doors are set to default values that cannot be changed, and the influence of the façade and building height should be taken into consideration in future work. Further research on image encoding methods and model optimization may also help to improve the prediction accuracy.

## 6. Conclusion

In this paper, a novel method is proposed for applying ResNet (CNN) and pix2pix (GAN) as metamodels for a daylight simulation, in order to predict the overall daylight performance metrics and visualization of the illuminances, respectively. The results of ResNet on two datasets prove the ability of CNNs to predict the daylight performance for general building forms instead of certain forms controlled by specific parameters. The best  $R^2$  of 0.959 and MSE of 0.008 were obtained on the real-case dataset for daylight uniformity. The prediction of static daylight metrics overperformed that of annual metrics on the same dataset and model structure. Larger datasets are needed to improve the prediction performance of annual metrics because the pattern is more complicated. The Geometric information is encoded as images, and CNNs can learn to extract features at different levels for a performance prediction, which provides a possible solution for a general proxy model that can be integrated into automatic performance-oriented form finding and design optimization. In addition, the visualization results of pix2pix validate the efficiency and effectiveness in predicting the illuminance distribution. A time cost within 1 s and a mean SSIM of 0.90 in test set can fulfill the requirements of real-time intuitive feedback for human designers to optimize the daylight performance. The two prediction models could

provide fast daylight predictions for general building forms without complex input parameters. Thus, they are suitable for the early design stage when details of the building components are hard to be specified, and the potential for a performance improvement mainly depends on the building form and indoor partition. Limitations of this study include model generalization on climates, building orientation, grid size and façade, which need further research.

## Declaration of competing interest

The authors declare that they have no known competing financial interests or personal relationships that could have appeared to influence the work reported in this paper.

## Acknowledgements

Dataset collection and annotation are supported by Beijing Institute of Residential Building Design & Research co, LTD.

This research is supported by the National Natural Science Foundation for Distinguished Young Scholars of China (NSFC, 51825802)

## References

- [1] C. Parmesan, G. Yohe, A globally coherent fingerprint of climate change impacts across natural systems, [J]. *Nature* 421 (6918) (2003) 37–42, <https://doi.org/10.1038/nature01286>.
- [2] Luis Pérez-Lombard, José Ortiz, C. Pout, A review on buildings energy consumption information[J], *Energy Build.* 40 (3) (2008) 394–398, <https://doi.org/10.1016/j.enbuild.2007.03.007>.

- [3] A.M. Omer, Energy, environment and sustainable development[J], Renew. Sustain. Energy Rev. 12 (9) (2008) 2265–2300, <https://doi.org/10.1016/j.rser.2007.05.001>.
- [4] J. Mardaljevic, L. Heschong, E. Lee, Daylight metrics and energy savings[J], Light. Res. Technol. 41 (3) (2011) 261–283, <https://doi.org/10.1177/1477153509339703>.
- [5] L. Bellia, A. Pedace, G. Barbato, Lighting in educational environments: an example of a complete analysis of the effects of daylight and electric light on occupants[J], Building and Environment, 2013, <https://doi.org/10.1016/j.buildenv.2013.04.005>.
- [6] M.L. Amundadottir, S. Rockcastle, M.S. Khanie, et al., A human-centric approach to assess daylight in buildings for non-visual health potential, visual interest and gaze behavior[J], Build. Environ. 113 (FEB) (2016) 5–21, <https://doi.org/10.1016/j.buildenv.2016.09.033>.
- [7] Z. Li, H. Chen, B. Lin, et al., Fast bidirectional building performance optimization at the early design stage[J], Building Simulation 11 (4) (2018) 647–661, <https://doi.org/10.1007/s12273-018-0432-1>.
- [8] C.F. Reinhart, O. Walkenhorst, Validation of dynamic RADIANCE-based daylight simulations for a test office with external blinds[J], Energy Build. 33 (7) (2001) 683–697, [https://doi.org/10.1016/S0378-7788\(01\)00058-5](https://doi.org/10.1016/S0378-7788(01)00058-5).
- [9] F. Christoph, Reinhart, et al., The simulation of annual daylight illuminance distributions — a state-of-the-art comparison of six RADIANCE-based methods[J], Energy Build. (2000), [https://doi.org/10.1016/S0378-7788\(00\)00042-6](https://doi.org/10.1016/S0378-7788(00)00042-6).
- [10] Reinhart Christoph, Pierre-Felix, et al., Experimental validation of Autodesk® 3ds Max® design 2009 and daysim 3.0[J], Leukos (2009), <https://doi.org/10.1582/LEUKOS.2009.06.01001>.
- [11] W. Zuo, A. McNeil, M. Wetter, E. Lee, Acceleration of Radiance for Lighting Simulation by Using Parallel Computing with OpenCL (No. LBNL-5094E), Lawrence Berkeley National Lab.(LBNL), Berkeley, CA (United States), 2011.
- [12] W. Zuo, A. McNeil, M. Wetter, E.S. Lee, Acceleration of the matrix multiplication of Radiance three phase daylighting simulations with parallel computing on heterogeneous hardware of personal computer, Journal of Building Performance Simulation 7 (2) (2014) 152–163.
- [13] N.L. Jones, C.F. Reinhart, Speedup potential of climate-based daylight modelling on GPUs, in: Building Simulation Conference, 2017, pp. 1438–1447.
- [14] T. Dogan, C. Reinhart, P. Michalatos, Urban daylight simulation calculating the daylit area of urban designs, Proceedings of SimBuild 5 (1) (2012) 613–620.
- [15] S. Müller, W. Kresse, N. Gatenby, F. Schöeffel, June). A radiosity approach for the simulation of daylight, in: Eurographics Workshop on Rendering Techniques, Springer, Vienna, 1995, pp. 137–146.
- [16] B. Geebelen, M. van der Voorden, H. Neuckermans, Fast and accurate simulation of long-term daylight availability using the radiosity method, Light. Res. Technol. 37 (4) (2005) 295–310.
- [17] P. Westermann, R. Evins, Surrogate modelling for sustainable building design – a review[J], Energy Build. 198 (2019) 170–186, <https://doi.org/10.1016/j.enbuild.2019.05.057>.
- [18] P. Geyer, S. Singaravel, Component-based machine learning for performance prediction in building design[J], Appl. Energy 228 (2018) 1439–1453, <https://doi.org/10.1016/j.apenergy.2018.07.011>.
- [19] M. Ayoub, A review on machine learning algorithms to predict daylighting inside buildings[J], Sol. Energy 202 (2020) 249–275, <https://doi.org/10.1016/j.solener.2020.03.104>.
- [20] Y. LeCun, Y. Bengio, G. Hinton, Deep learning, Nature 521 (2015) 436–444, <https://doi.org/10.1038/nature14539>.
- [21] S. Pouyanfar, S. Sadiq, Y. Yan, et al., A survey on deep learning: algorithms, techniques, and applications[J], ACM Comput. Surv. 51 (5) (2018) 1–36, <https://doi.org/10.1145/3234150>.
- [22] Alex Krizhevsky, Ilya Sutskever, Geoffrey E. Hinton, ImageNet classification with deep convolutional neural networks, in: Proceedings of the 25th International Conference on Neural Information Processing Systems, ume 1, (NIPS'12). Curran Associates Inc., Red Hook, NY, USA, 2012, pp. 1097–1105, <https://doi.org/10.1145/3065386>.
- [23] N.L. Jones, C.F. Reinhart, Effects of real-time simulation feedback on design for visual comfort[J], Journal of Building Performance Simulation (2018) 1–19, <https://doi.org/10.1080/19401493.2018.1449889>.
- [24] Ian J. Goodfellow, Jean Pouget-Abadie, Mehdi Mirza, Bing Xu, David Warde-Farley, Sherjil Ozair, Aaron Courville, Yoshua Bengio, Generative adversarial nets. NIPS'14), in: Proceedings of the 27th International Conference on Neural Information Processing Systems -, ume 2, MIT Press, Cambridge, MA, USA, 2014, pp. 2672–2680.
- [25] A. Creswell, T. White, V. Dumoulin, et al., Generative adversarial networks: an overview[J], IEEE Signal Process. Mag. 35 (1) (2017) 53–65, <https://doi.org/10.1109/MSP.2017.2765202>.
- [26] S. Li, L. Liu, C. Peng, A review of performance-oriented architectural design and optimization in the context of sustainability: dividends and challenges[J], Sustainability 12 (2020), <https://doi.org/10.3390/su12041427>.
- [27] D.O. Economics, U.O. Wisconsin, Using Randomization to Break the Curse of Dimensionality[C], EconWPA, 1996.
- [28] Y. Bengio, O. Delalleau, N. Le Roux, The curse of highly variable functions for local kernel machines, Proc. Advances in Neural Information Processing Systems 18 (2005) 107–114.
- [29] M. Beccali, M. Bonomolo, G. Ciulla, et al., Assessment of indoor illuminance and study on best photosensors' position for design and commissioning of Daylight Linked Control systems. A new method based on artificial neural networks[J], Energy 154 (JUL.1) (2018) 466–476, <https://doi.org/10.1016/j.energy.2018.04.106>.
- [30] Hu Jia, Svetlana Olbina, Illuminance-based slat angle selection model for automated control of split blinds[J], Build. Environ. 46 (3) (2011) 786–796.
- [31] V. Logar, Z. Kristl, I. Skrjanc, Using a fuzzy black-box model to estimate the indoor illuminance in buildings[J], Energy Build. 70 (feb) (2014) 343–351, <https://doi.org/10.1016/j.enbuild.2013.11.082>.
- [32] Tuğçe Kazanasmaz, Murat Günaydin, Selcen Binol, Artificial neural networks to predict daylight illuminance in office buildings, Build. Environ. 44 (Issue 8) (2009) 1751–1757, <https://doi.org/10.1016/j.buildenv.2008.11.012>. ISSN 0360-1323.
- [33] Y. Liu, A. Colburn, M. Inanici, Computing long-term daylighting simulations from high dynamic range imagery using deep neural networks[C], in: 2018 Building Performance Analysis Conference and SimBuild, 2018.
- [34] M. Inanici, Computing Long-Term Daylighting Simulations from High Dynamic Range Imagery Using Deep Neural Networks[D], 2019.
- [35] I. Chatzikostantinou, S. Sarıyıldız, Approximation of simulation-derived visual comfort indicators in office spaces: a comparative study in machine learning[J], Architect. Sci. Rev. 59 (4) (2016) 1–16, <https://doi.org/10.1080/00038628.2015.1072705>.
- [36] A. Ahmed, N.E. Korres, J. Ploennigs, et al., Mining building performance data for energy-efficient operation[J], Adv. Eng. Inf. 25 (2) (2011) 341–354, <https://doi.org/10.1016/j.aei.2010.10.002>.
- [37] A. Ahmed, M. Otreba, N.E. Korres, et al., Assessing the performance of naturally day-lit buildings using data mining[J], Adv. Eng. Inf. 25 (2) (2011) 364–379, <https://doi.org/10.1016/j.aei.2010.09.002>.
- [38] E. Nault, P. Moonen, E. Rey, et al., Predictive models for assessing the passive solar and daylight potential of neighborhood designs: a comparative proof-of-concept study - ScienceDirect[J], Build. Environ. 116 (2017) 1–16, <https://doi.org/10.1016/j.buildenv.2017.01.018>.
- [39] V.R.M. Lo Verso, G. Mihaylov, A. Pellegrino, et al., Estimation of the daylight amount and the energy demand for lighting for the early design stages: definition of a set of mathematical models[J], Energy Build. 155 (nov) (2017) 151–165, <https://doi.org/10.1016/j.enbuild.2017.09.014>.
- [40] Clara-Larissa Lorenz, Michael Packianather, A. Benjamin Spaeth, Clarice Bleil De Souza, Artificial neural network-based modelling for daylight evaluations, in: Proceedings of the Symposium on Simulation for Architecture and Urban Design, Society for Computer Simulation International, San Diego, CA, USA, 2018, <https://doi.org/10.22360/simaud.2018.simaud.002>. Article 2, 1–8.
- [41] M. Ayoub, A multivariate regression to predict daylighting and energy consumption of residential buildings within hybrid settlements in hot-desert climates[J], Indoor Built Environ. 28 (6) (2019) 848–866, <https://doi.org/10.1177/1420326X18798164>.
- [42] Linhai SHEN, YUNSONG Han, Comparative analysis of machine learning models optimized by bayesian algorithm for indoor daylight distribution prediction by bayesian algorithm for indoor daylight distribution prediction[C], in: 35th PLEA CONFERENCE SUSTAINABLE ARCHITECTURE and URBAN DESIGN Planning Post Carbon Cities, 2020.
- [43] B. Dong, V. Prakash, F. Feng, et al., A review of smart building sensing system for better indoor environment control[J], Energy Build. 199 (SEP.) (2019) 29–46, <https://doi.org/10.1016/j.enbuild.2019.06.025>.
- [44] H. Saha, A.R. Florita, G.P. Henze, et al., Occupancy sensing in buildings: a review of data analytics approaches[J], Energy Build. 188–189 (APR) (2019) 278–285, <https://doi.org/10.1016/j.enbuild.2019.02.030>.
- [45] K. Sun, Q. Zhao, J. Zou, A review of building occupancy measurement systems[J], Energy Build. 216 (2020) 109965, <https://doi.org/10.1016/j.enbuild.2020.109965>.
- [46] A A K M, B J D, C T K, et al., A novel occupancy detection solution using low-power IR-FPA based wireless occupancy sensor - ScienceDirect[J], Energy Build. 192 (2019) 63–74, <https://doi.org/10.1016/j.enbuild.2019.03.022>.
- [47] A J Y, A A P, A K A C, et al., Comparison of different occupancy counting methods for single system-single zone applications[J], Energy Build. 172 (2018) 221–234, <https://doi.org/10.1016/j.enbuild.2018.04.051>.
- [48] S. Petersen, T.H. Pedersen, K.U. Nielsen, et al., Establishing an image-based ground truth for validation of sensor data-based room occupancy detection[J], Energy Build. 130 (oct) (2016) 787–793, <https://doi.org/10.1016/j.enbuild.2016.09.009>.
- [49] Huang-Chia Shih, A robust occupancy detection and tracking algorithm for the automatic monitoring and commissioning of a building, Energy Build. 77 (2014) 270–280, <https://doi.org/10.1016/j.enbuild.2014.03.069>. ISSN 0378-7788.
- [50] Jianhong Zou, Qianchuan Zhao, Yang Wen, Fulin Wang, Occupancy detection in the office by analyzing surveillance videos and its application to building energy conservation, Energy Build. 152 (2017) 385–398, <https://doi.org/10.1016/j.enbuild.2017.07.064>. ISSN 0378-7788.
- [51] C. Zhenghua, J. Chaoyang, Building occupancy modeling using generative adversarial network[J], Energy Build. 174 (2018) 372–379, <https://doi.org/10.1016/j.enbuild.2018.06.029>.
- [52] P.W. Tiern, S. Wei, J.K. Calautit, et al., A vision-based deep learning approach for the detection and prediction of occupancy heat emissions for demand-driven control solutions[J], Energy Build. (2020) 110386, <https://doi.org/10.1016/j.enbuild.2020.110386>.
- [53] Meng Y B, Li T Y , Liu G H , et al. Real-time dynamic estimation of occupancy load and an air-conditioning predictive control method based on image information fusion - ScienceDirect[J]. Build. Environ., 173. <https://doi.org/10.1016/j.buildenv.2020.106741>.
- [54] D. Gonzalez, D. Rueda-Plata, A.B. Acevedo, et al., Automatic detection of building typology using deep learning methods on street level images[J], Build. Environ. 177 (2020) 106805, <https://doi.org/10.1016/j.buildenv.2020.106805>.

- [56] Wang Zhoutong, et al., Quantifying legibility of indoor spaces using Deep Convolutional Neural Networks: case studies in train stations[J], *Build. Environ.* (2019), <https://doi.org/10.1016/j.buildenv.2019.04.035>.
- [57] S. Tarabishi, S. Psarras, M. Kosicki, et al., Deep learning surrogate models for spatial and visual connectivity[J], *Int. J. Architect. Comput.* (2019), <https://doi.org/10.1177/1478077119894483>.
- [58] I. Ha, H. Kim, S. Park, et al., Image retrieval using BIM and features from pretrained VGG network for indoor localization[J], *Build. Environ.* (2018) 23–31, <https://doi.org/10.1016/j.buildenv.2018.05.026>.
- [59] L. De Baets, J. Ruyssinck, C. Develder, et al., Appliance classification using VI trajectories and convolutional neural networks[J], *Energy Build.* 158 (PT.1) (2018) 32–36, <https://doi.org/10.1016/j.enbuild.2017.09.087>.
- [60] J. Loy-Benitez, S.K. Heo, C.K. Yoo, Imputing Missing Indoor Air Quality Data via Variational Convolutional Autoencoders: Implications for Ventilation Management of Subway Metro systems[J], *Building and Environment*, 2020, p. 107135, <https://doi.org/10.1016/j.buildenv.2020.107135>.
- [61] S. Ghimire, R.C. Deo, N. Raj, et al., Deep solar radiation forecasting with convolutional neural network and long short-term memory network algorithms[J], *Appl. Energy* 253 (NOV.1) (2019) 113541, <https://doi.org/10.1016/j.apenergy.2019.113541>, 1-113541.20.
- [62] Z. Han, Z. Yuxun, Y. Jianfei, et al., Towards occupant activity driven smart buildings via WiFi-enabled IoT devices and deep learning[J], *Energy Build.* (2018), <https://doi.org/10.1016/j.enbuild.2018.08.010>. S037877881831329X..
- [63] A K Y , B J H , C W S , et al. Unsupervised learning for fault detection and diagnosis of air handling units[J]. *Energy Build.*, 210. <https://doi.org/10.1016/j.enbuild.2019.109689>.
- [64] K. Yan, A. Chong, Y. Mo, Generative adversarial network for fault detection diagnosis of chillers[J] 172, *Building and Environment*, 2020, p. 106698, <https://doi.org/10.1016/j.buildenv.2020.106698>.
- [65] Z. Wang, T. Hong, Generating realistic building electrical load profiles through the Generative Adversarial Network[J], *Energy Build.* 224 (2020), <https://doi.org/10.1016/j.enbuild.2020.110299>.
- [66] A. Tijskens, S. Roels, H. Janssen, Neural networks for metamodelling the hygrothermal behaviour of building components[J], *Build. Environ.* 162 (Sep) (2019) 106282, <https://doi.org/10.1016/j.buildenv.2019.106282>, 1-106282.11.
- [67] A Y G , A Y R , A C F , et al. Deep learning and transfer learning models of energy consumption forecasting for a building with poor information data[J]. *Energy Build.*, 223. <https://doi.org/10.1016/j.enbuild.2020.110156>.
- [68] Mateus Dias Ribeiro, Abdul Rehman, Sheraz Ahmed, Andreas Dengel, *DeepCFD: Efficient Steady-State Laminar Flow Approximation with Deep Convolutional Neural Networks*, 2020, 08826 arXiv:2004.
- [69] Songlin Xiang, Xiangwen Fu, Jingcheng Zhou, et al., Non-intrusive reduced order model of urban airflow with dynamic boundary conditions[J], *Build. Environ.* 187 (2021), 107397, <https://doi.org/10.1016/j.buildenv.2020.107397>.
- [70] Theodore Galanos, DaylightGAN. <https://github.com/TheodoreGalanos/DaylightGAN>, 2020.
- [71] K. He, X. Zhang, S. Ren, et al., Deep residual learning for image recognition[J]. <https://doi.org/10.1109/CVPR.2016.90>, 2016.
- [72] K. He, X. Zhang, S. Ren, et al., Identity mappings in deep residual networks[J]. [https://doi.org/10.1007/978-3-319-46493-0\\_38](https://doi.org/10.1007/978-3-319-46493-0_38), 2016.
- [73] Phillip Isola, Jun-Yan Zhu, Tinghui Zhou, A. Alexei, Efros. Image-To-Image Translation with Conditional Adversarial Networks, *CVPR*, 2017, <https://doi.org/10.1109/CVPR.2017.632>.
- [74] A. Radford, L. Metz, S. Chintala, *Unsupervised representation learning with deep convolutional generative adversarial networks*, *ICLR* 2 (3) (2016) 16.
- [75] S.J. Pan, Q. Yang, A survey on transfer learning[J], *IEEE Trans. Knowl. Data Eng.* 22 (10) (2010) 1345–1359, <https://doi.org/10.1109/TKDE.2009.191>.
- [76] W. Zhou, A.C. Bovik, H.R. Sheikh, et al., Image quality assessment: from error visibility to structural similarity[J], *IEEE Trans. Image Process.* 13 (4) (2004), <https://doi.org/10.1109/TIP.2003.819861>.
- [77] V.D.W. Kevin, M. Inanici, A critical investigation of common lighting design metrics for predicting human visual comfort in offices with daylight[J], *LEUKOS The Journal of the Illuminating Engineering Society of North America* 10 (1–4) (2014) 145–164, <https://doi.org/10.1080/15502724.2014.881720>.
- [78] C.F. Reinhart, J. Mardaljevic, Z. Rogers, Dynamic daylight performance metrics for sustainable building design[J], *Leukos* 3 (1) (2006) 7–31, <https://doi.org/10.1582/LEUKOS.2006.03.01.001>.
- [79] A. Nabil, J. Mardaljevic, Useful daylight illuminances: a replacement for daylight factors[J], *Energy Build.* 38 (7) (2006) 905–913, <https://doi.org/10.1016/j.enbuild.2006.03.013>.
- [80] ClimateStudio: <https://www.solemma.com/climatestudio>.